Dry Intrusions Following Eastward-Propagating Synoptic-Scale Cloud Systems over Sumatera Island

Fumie MURATA

Research Institute for Humanity and Nature, Kyoto, Japan

Manabu D. YAMANAKA

Graduate School of Science and Technology, Kobe University, Kobe, Japan
Institute of Observational Research for Global Change, Japan Agency for Marine-Earth Science and Technology, Yokosuka, Japan

Hiroyuki HASHIGUCHI

Research Institute for Sustainable Humanosphere, Kyoto University, Kyoto, Japan

Shuichi MORI

Institute of Observational Research for Global Change, Japan Agency for Marine-Earth Science and Technology, Yokosuka, Japan

Mahally KUDSY, Tien SRIBIMAWATI

Agency for the Assessment and Application of Technology, Jakarta Pusat, Indonesia

Budi SUHARDI and EMRIZAL

Indonesian Meteorological and Geophysical Agency, Jakarta Pusat, Indonesia

(Manuscript received 20 April 2005, in final form 16 November 2005)

Abstract

We observed four dry intrusions that occurred over Sumatera Island (Sumatra) during the intensive rawinsonde observation periods in 1998–2004. The events were accompanied by westerly winds, and included the passage of a single organized synoptic-scale cloud system, with a structure similar to a squall line. The cloud systems had the properties of a Kelvin wave. Eastward propagation speed was around 13 m/s, and the horizontal scale was several thousand kilometers. Severe rain occurred as the cloud systems passed, and dry intrusion suppressed convections in the rear part.

1. Introduction

Some of the most active convection in the world occurs around Indonesia (e.g., Ramage 1968; Webster and Lucas 1992). Warm sea surface temperatures provide sufficient water vapor throughout the year. The complex land-sea

Corresponding author: Fumie Murata, Research Institute for Humanity and Nature 457-1, Kamigamo Motoyama, Kita-ku, Kyoto 603-8047, Japan.
E-mail: murataf@chikyu.ac.jp

distribution over Indonesia supports local land-sea breeze circulations (Hadi et al. 2000, 2002). Complex topography supports mountain-valley winds. Convergence occurs over mountains, between islands, or with background winds (Houze et al. 1980). Many studies have remarked on the dominance of the diurnal variation in convection (e.g., Murakami 1983; Hendon and Woodberry 1993; Nitta and Sekine 1994; Yang and Slingo 2001). Sui and Lau (1992) analyzed satellite data and noted that convection on diurnal cycle diminished during the active phase of the Madden-Julian Oscillation (MJO; Madden and Julian 1971, 1972, 1994). However, detailed analyses using in situ observations have not been conducted. In this paper, we focus on the suppression of convection on intraseasonal timescales, using in situ observations.

Dry intrusions can suppress convection (e.g., Numaguti et al. 1995; Brown and Zhang 1997; DeMott and Rutledge 1998). Dry intrusions were first recognized and investigated in observations from the Tropical-Ocean Global-Atmosphere Coupled Ocean-Atmosphere Response Experiment (TOGA COARE; Webster and Lucas 1992). Dry intrusions are characterized by very dry air in the lower or middle troposphere (e.g., Parsons et al. 1994). Vertical air parcel displacement cannot explain the dryness of air; instead, lateral advection is responsible (Numaguti et al. 1995; Mapes and Zuidema 1996). Horizontal distributions of precipitable water (PW) derived from satellite data confirm the dry air advection that forces the remarkable decrease in humidity in the humid lower troposphere (e.g., Sheu and Liu 1995). Back-trajectory analyses using objective analysis data also show the dry air advection from the subtropics or mid-latitudes (e.g., Yoneyama and Fujitani 1995; Yoneyama and Parsons 1999). Two factors facilitate convective suppression in dry intrusions: entrainment of dry air, and the suppression of vertical motion by a stable layer at the base of the dry layer (Numaguti et al. 1995; Mapes and Zuidema 1996).

Dry intrusions in the western Pacific have been observed and analyzed since TOGA COARE (Yoneyama 2003), but few studies have detailed dry intrusions in the Indian Ocean or over Indonesia. Yatagai and Sumi (1997) used only satellite data, and reported dry intrusions over the Indian and Pacific Oceans. Zachariasse et al. (2001) reported very dry air in the middle troposphere over the Indian Ocean.

Several studies (e.g., Parsons et al. 2000; Johnson et al. 2001; Redelsperger et al. 2002) suggested that convective suppression, and subsequent remoistening in the boundary layer and free atmosphere, may regulate MJO. However, few studies related dry intrusions to cloud systems. The dry intrusions described in this study were related to eastward-propagating synoptic-scale cloud systems.

Eastward-propagating synoptic-scale cloud systems were described by Nakazawa (1986, 1988), Takayabu and Murakami (1991), and Dunkerton and Crum (1995). These cloud systems have been also studied as convectively coupled Kelvin waves using spectral analysis (e.g., Takayabu 1994; Wheeler and Kiladis 1999; Wheeler et al. 2000). Nakazawa (1986, 1988) described how the cloud systems were related to the MJO, and called them super-clusters. But, such disturbances have been observed independent of the MJO (Takayabu and Murakami 1991; Dunkerton and Crum 1995).

Here, we describe dry intrusions that were observed over the province of West Sumatera, located near the Equator on the west coast of Sumatera Island (Fig. 1). Data were provided by several intensive rawinsonde observation periods that were conducted over Sumatera (Murata et al. 2002; Mori et al. 2004; Sakurai et al. 2005). We investigated four dry events that occurred during the intensive rawinsonde observation periods. In this paper, we describe common features of the four observed dry events. Section 2 describes the data used. Observations for each case are discussed in Section 3. Composite analyses are examined in Section 4, including background conditions (Section 4.1) and observational results (Section 4.2). Analyses are compared with past studies and discussed in Section 5. Section 6 contains the conclusion.

2. Data

1) Observation sites and periods:

Rawinsonde data, and surface meteorological data were observed at two stations (Fig. 1) in the province of West Sumatera, Sumatera Island, Indonesia. Coordinated universal time

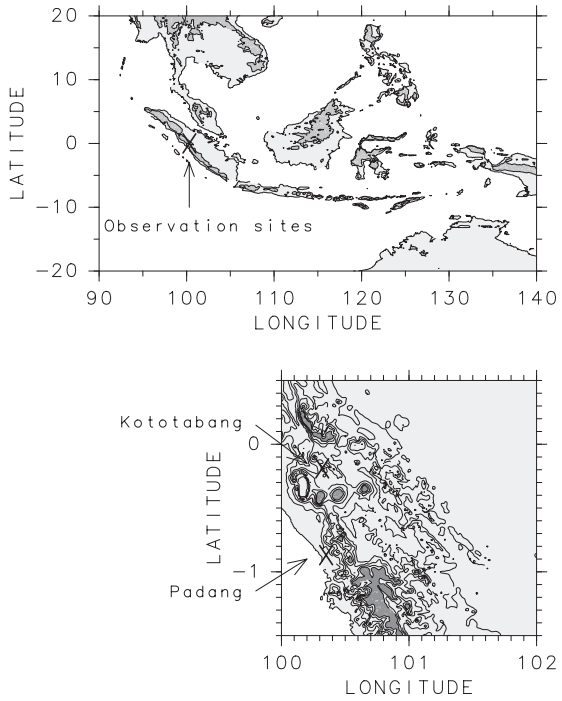

Fig. 1. Location of observation sites: Kototabang and Padang. Light shading shows land region. Dark shading in the upper and lower figures shows altitudes more than 500 m, and that more than 1500 m, respectively. Contours in the lower figure are drawn every 250 m up to 1500 m.

(UTC), and mean sea level (MSL) are used to depict time and height, respectively, in this study. Local standard time (LST) at both sites is UTC + 7 hours. 'Kototabang' (100.32°E, 0.20°S, 865 m MSL) is in the mountains, about 50 km from the west coast of Sumatera. 'Padang' (100.35°E, 0.88°S, 2 m MSL) is a port town on the Indian Ocean. Three intensive rawinsonde observation periods (4–7 October 1998, 27–31 May 2001, and 6–12 June 2001) at Kototabang, and one intensive rawinsonde observation period (5–9 May 2004) at Padang were analyzed.

2) Rawinsondes:

Rawinsondes were launched four times daily (00, 06, 12, and 18 UTC) at Kototabang, and twice daily (00 and 12 UTC) at Padang. AIR company rawinsondes were used for soundings in 1998. Vaisala rawinsondes were used in 2001 and 2004. The Vaisala rawinsondes included new RS80-15GH, and old RS80-15G models. The old RS80-15G models recorded soundings in 2004. Past studies (e.g., Fujiwara et al. 2003; Nakamura et al. 2004) have noted a dry bias at lower altitudes in data from RS80-15G models. Therefore, a humidity correction was applied as described in the Appendix. TA1000 and TX1000 1000-g meteorological balloons from the TOTEX Company were used. TX1000 balloons were used at night (12, 18 UTC or 19, 01 LST) to minimize balloon burst near the tropopause. Analyzed data included temperature, relative humidity, pressure, and zonal winds; all were averaged every 100 m.

3) Surface data:

Hourly pressure, temperature, and relative humidity in 1998 and 2004 were provided by standard operational surface observations (barograph and thermohygrograph) at stations of the Indonesian Meteorological and Geophysical Agency (BMG), where the intensive rawinsonde observations were conducted. Rainfall data in 1998 were observed by a standard tipping-bucket-type rain gauge (Ogasawara Company) with resolutions of 0.5 mm and 1 min. An accumulation-type rain gauge measured 3-hourly rainfall data in 2004. The latter was a routine observation that was provided by BMG. A Vaisala automatic weather station (MAWS201) measured surface data in 2001. MAWS201 comprised a PMT16A pressure sensor, QMH101 temperature and humidity sensors, and a QMR101 precipitation sensor. The original time resolution of MAWS201 is 1 min for hourly averaged surface pressure, temperature and relative humidity, and 6-hourly (00, 06, 12, 18 UTC) accumulated rainfall data. The 6-hourly rainfall values were accumulations from the previous six hours.

4) Black body temperature from satellite:

The black body temperature (T_{BB}) data used were observed by Geostationary Meteorological Satellite in 1998 and 2001, and by GOES-9 in 2004. All data were provided by Kochi University. Hourly data were used with horizontal resolution of 0.5° in longitude and latitude.

5) Precipitable water by satellite:

A precipitable water (PW) dataset from SSM/I(F14) was provided by Remote Sensing

Systems[1]. The dataset was a 3-day average of the previous day, the present day, and the next day, with a horizontal resolution of 0.5° in longitude and latitude.

6) Objective analysis data:

Data used were from the NCEP/NCAR reanalysis (Kalnay et al. 1996) and included zonal wind, meridional wind, and omega. Data were 6-hourly values, with a horizontal resolution of 2.5° in longitude and latitude.

3. Case study

Each of four dry events, and the accompanying background conditions are described in this section. These events had relative humidities of less than 50% in the lower troposphere up to 6 km; the dryness persisted for more than half a day. MJO active phases noted were defined by negative periods of 20–70-days filtered T_{BB} for 80–100°E, and 10°N–10°S averaged data.

Figure 2a is a time-longitude section of T_{BB}, averaged between 0 and 1°S during 4–7 October 1998. The days shown in the figure were after the end of an active MJO phase, but high cloud developed in the eastern Indian Ocean. Convection was active in the Indian Ocean during the first 2 days. The dotted line denotes an eastward propagating speed of 10°/day or 13 m/s. T_{BB} colder than 220 K appeared at 87°E at 06 UTC, and at 93°E at 18 UTC 4 October, and subsequently propagated eastward at about 13 m/s. After the cloud system passed across 100°E, the cloud tops became lower, or the region of high cloud tops became smaller than the west. Eastward propagation was discrete in 100–107°E, and became indistinct near 110°E. Rains fell during 00–18 UTC (07–01 LST of the following day) on 4 October, and 06–24 UTC (13–07 LST of the following day) on 5 October (Fig. 2b). Figure 2c shows a time-height section of 6-hourly zonal winds up to 6 km. Strong westerly winds exceeding 10 m/s began at 12 UTC on 5 October, corresponding to the passage of an eastward-propagating cloud system. The top of the layer of westerly winds exceeding 10 m/s rose from 3 km to 5 km between 5 and 7 October. Figure 2d shows a time-height section of 6-hourly relative humidity up to 10 km. Humidity exceeding 80% extended up to 10 km between 12 and 18 UTC (19 and 01 LST of the following day) on 5 October as the cloud system passed. A region of high humidity between 5 and 8 km persisted until

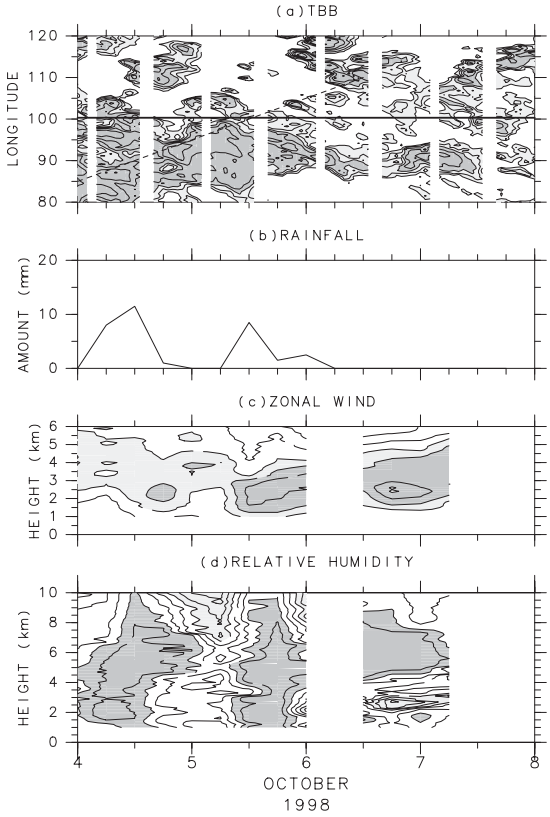

Fig. 2. (a) Time-longitude section of hourly T_{BB} averaged between 0 and 1°S during 4–7 October 1998. Dark and light shading indicates T_{BB} colder than 240 K, 260 K, respectively. The contour interval is 10 K. A solid line of 100.3°E shows the observation site. A dotted line represents a reference speed of 10°/day or 13 m/s. (b) Timeseries of 6-hourly rainfall amount. The rainfall amounts represent accumulation during the previous 6 hours. (c) Time-height section of 6-hourly zonal wind. Dark and light shading indicates zonal winds more than 10 m/s and 5 m/s, respectively. A contour interval is 5 m/s. (d) Time-height section of 6-hourly relative humidity. Dark and light shading indicates relative humidity exceeding 80%, and less than 50%, respectively. A contour interval is 10%.

1 www.remss.com

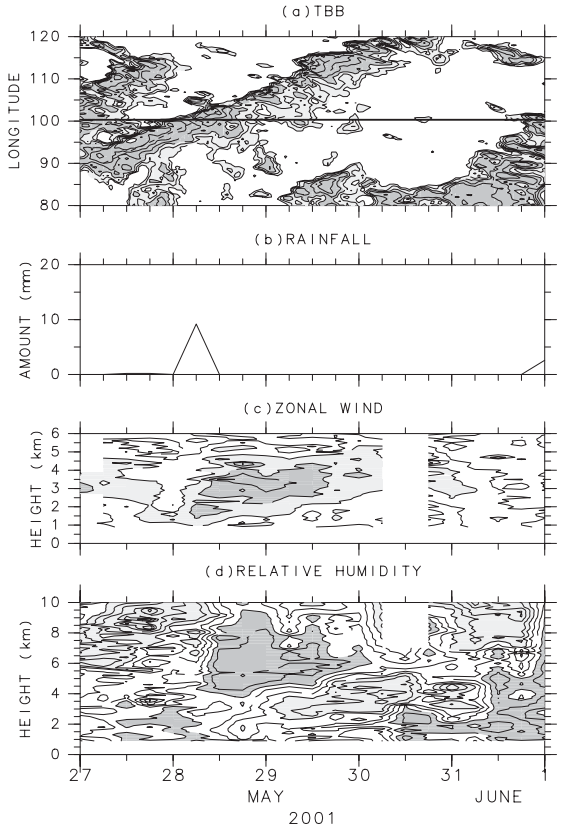

Fig. 3. Same as Fig. 2 except for 27–31 May 2001.

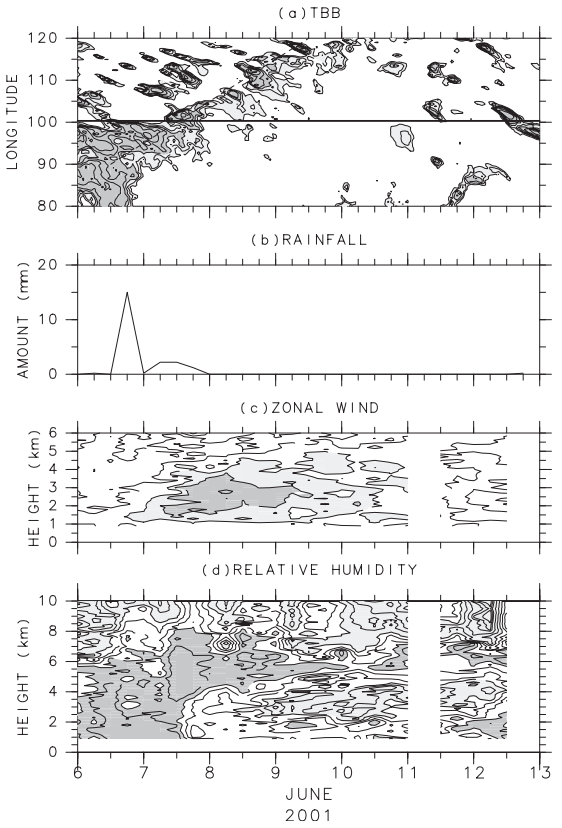

Fig. 4. Same as Fig. 2 except for 6–12 June 2001.

the end of the sounding period. From 6 October, the bottom of the humid layer corresponded to the upper boundary of strong westerly winds. Dry air with relative humidity less than 50%, appeared at around 2 km at 00 UTC on 6 October, and persisted during 18 UTC on 6 October–06 UTC on 7 October at 2–3 km in the layer with westerly winds.

Figure 3 is similar to Fig. 2, and shows a dry event between 27 and 31 May 2001. The period corresponded to the beginning of an active MJO phase. Convection in the Indian Ocean reactivated after 31 May. There were some similarities to the 1998 case shown in Fig. 2. For example, a synoptic-scale cloud system propagated eastward at around 13 m/s through the observation site. Lower-tropospheric westerlies strengthened as the cloud system passed. The layer of westerly winds became gradually dry and dry air lower than 50% appeared in the following day. This dry westerly layer ascended around 1 km/day. Air with high relative humidity overlays the dry layer.

There are also some differences between Fig. 3 and Fig. 2. The cloud propagating to the east between 90 and 120°E (Fig. 3a) was distinct, maintaining during its propagation a zonal scale of around 1,000 km for T_{BB} colder than 260 K. Propagation speed was slightly slower than 13 m/s. Rainfall was observed in the morning (00–06 UTC or 07–13 LST; Fig. 3b), but high humidity exceeding 80% was confined up to 4 km. Humidity exceeding 80% appeared above 5 km at 12 UTC (19 LST) on 28 May. Dry air lower than 50% appeared 1 day after the onset of westerly wind exceeding 10 m/s, and persisted for 2 days. Humidity exceeding 80% developed under the dry layer and extended up to 3 km at 12 UTC (19 LST) on 30 May and up to 7 km at 12 UTC (19 LST) on 31 May.

Figure 4 is similar to Figs. 2 and 3, and

shows the dry event of 6–12 June 2001. This period corresponded to the end of an active MJO phase. All similarities discussed in the previous case also apply to this one. Convection was active in the Indian Ocean during the first 2 days (Fig. 4a). An eastward-propagating cloud system was embedded within the high cloud cover over the Indian Ocean. As it passed over Indonesia, the cloud system comprised a discrete group of westward-propagating cloud systems with a lifetime of less than 24 hours. Rains fell during 12 and 18 UTC (19 and 01 LST of the following day) on 6 June. Lighter rains continued until 18 UTC (01 LST of the following day) on 7 June (Fig. 4b). Humidity exceeding 80% occurred in the lower troposphere (below 6 km) before the cloud system passed through (Fig. 4d). After the system had passed, humidity exceeded 80% between 4 and 8 km, persisting until 12 June. Humidity drier than 50% appeared 1 day after the onset of strong westerly winds. The dry air then persisted for 4 days. Humidity below the dry layer began to increase from 18 UTC (01 LST of the following day) on 11 June, and rainfall with thunder occurred near the observation site during 12–24 UTC (19–07 LST of the following day) of 12 June.

Figure 5 shows the dry event of 5–9 May 2004. Note that the observation site differed from the previous cases. The time resolution in Figs. 5c and 5d is 12 hours; otherwise, the figure is the same as Fig. 2. The period corresponds to the end of an active MJO phase. Convection in the Indian Ocean was active during the period (Fig. 5a), but the convection seemed to propagate both eastward and westward. Two eastward-propagating cloud systems were identified. Some clouds that merged together comprised cloud systems propagating westward. Precipitation fell between 06 and 12 UTC (13 and 19 LST) on 5 May, and again from 06–12 UTC (13–19 LST) on 6 May (Fig. 5b). Heavy rainfall (100 mm in 6 hours) occurred on 5 May 2004. In addition, wind gusts occurred before and during rainfall on 5 and 6 May. The westerly wind strengthened at 1 km at 12 UTC on 5 May as the first cloud system passed (Fig. 5c). Winds re-intensified at 12 UTC on 6 May, as the second cloud system passed, at which time strong westerlies appeared at 2–3 km. Westerly winds stronger than 10 m/s persisted

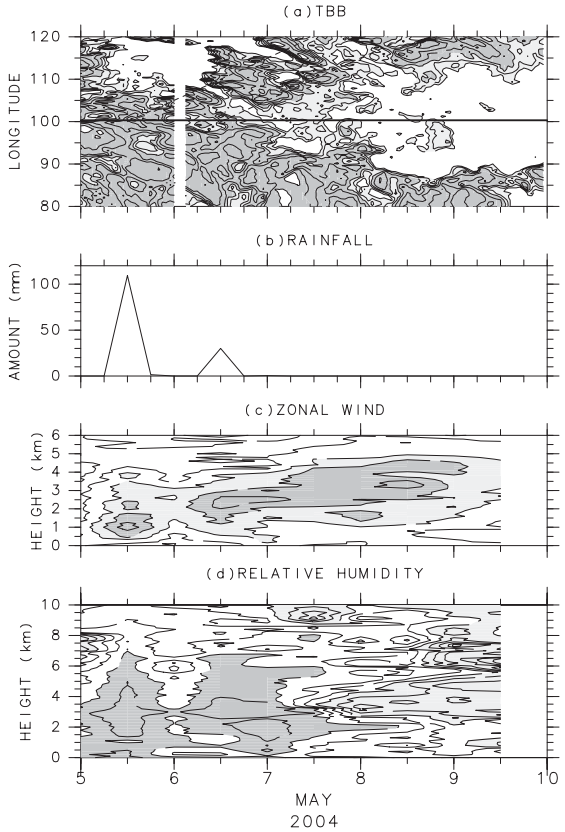

Fig. 5. Same as Fig. 2 except for 5–9 May 2004.

for 3 days, longer than in the other cases. The dry layer was 0.5 km higher than in the other cases. The humid layer which overlie the dry layer were 60–70%: lower than in the other cases, possibly because humidity correction was not applied above 5 km (see Appendix).

4. Composite analysis

A composite analysis extracted features common to the dry events described in Section 3. A composite was made for each onset day, i.e., the day on which westerly winds exceeded 10 m/s at 3 km. Onset days were 5 October 1998; 28 May 2001; 7 June 2001, and 6 May 2004. The analysis period was Day−1 (the day before the onset of strong westerly winds) to Day+3 (3 days after the onset of strong westerly winds).

4.1 Background condition

Figure 6 shows the horizontal distributions of composite T_{BB} and NCEP zonal winds, at 700 hPa from Day−1 to Day+3. Composites of

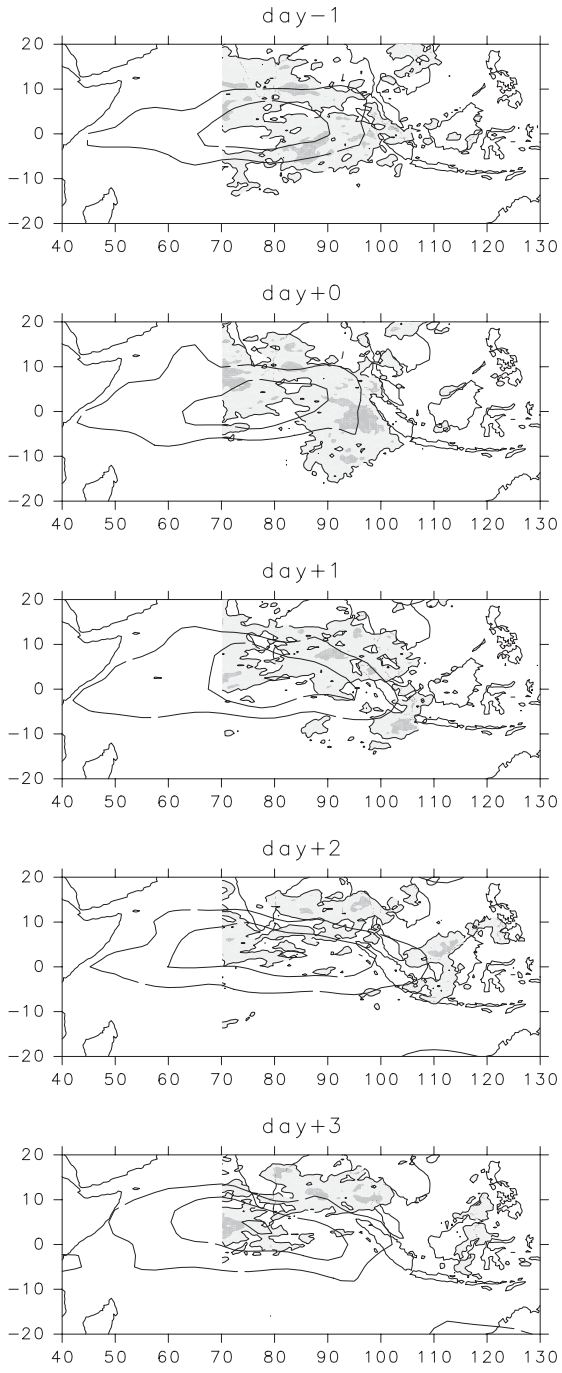

Fig. 6. Horizontal distributions of composite T_{BB} (shade) and NCEP zonal wind at 700 hPa (contour) from Day−1 to Day+3. Composites of T_{BB} in each figure were made from data observed on 00 UTC. Shading shows deep convection where T_{BB} were colder than 230 K (dark shading) and 250 K (light shading). Thick contours represent westerly winds of 5, 10, and 15 m/s.

T_{BB} in each figure were made from data observed at 00 UTC. Westerly winds prevailed over the equatorial Indian Ocean, and were stationary during Day−1 and Day+3. The core of the westerly winds was near (80°E, 2.5°N). The eastern edge of strong westerly wind, more than 5 m/s, extended eastward from Day+0 to Day+2, following the cloud system near the Equator, and retreated from Indonesia on Day+3.

Deep convection occurred over the eastern Indian Ocean on Day−1. There were cloud tops cooler than 230 K between 85 and 90°E on Day−1, which moved to within several tens of kilometers from the west coast of Sumatera on Day+0. The cloud systems near the Equator continued moving to the east, reaching the east coast of the Malay Peninsula, the east coast of Sumatera, and southwest of Jawa Island (Java) on Day+1. By Day+2, the cloud system near the Equator propagated farther east, over western Kalimantan Island (Borneo). The cloud system extended latitudinally from 10°S–10°N, and by Day+3, it was over the east coast of Kalimantan. High clouds over the equatorial Indian Ocean were not present until Day+3. The cloud systems over the Bay of Bengal also moved northward from Day+0 to Day+2.

Figure 7 shows the horizontal distributions of composite SSM/I PW and NCEP horizontal winds at 700 hPa from Day−1 to Day+3. The 700-hPa wind field shows a typical Matsuno-Gill pattern (Matsuno 1966; Gill 1980), with westerly winds over the equatorial Indian Ocean and western Indonesia, and easterly winds over eastern Indonesia, and Rossby gyres centered at 15°N and 7.5°S, straddling the Equator. Structure of the Matsuno-Gill pattern was almost stationary during Day−1 and Day+3.

PW exceeding 55 mm covered the eastern Indian Ocean and Indonesia, and relatively low PW (40–50 mm) was observed over the equatorial western Indian Ocean on Day−1. Low PW around 80°E intruded to the east at the center of strong westerly winds. The 55-mm isopleth of PW reached Sumatera on Day+1 and then decreased below 53 mm on Day+2. PW over the sea between Sumatera and Kalimantan Islands dropped below 55 mm on Day+3. The westerly wind weakened over Sumatera on

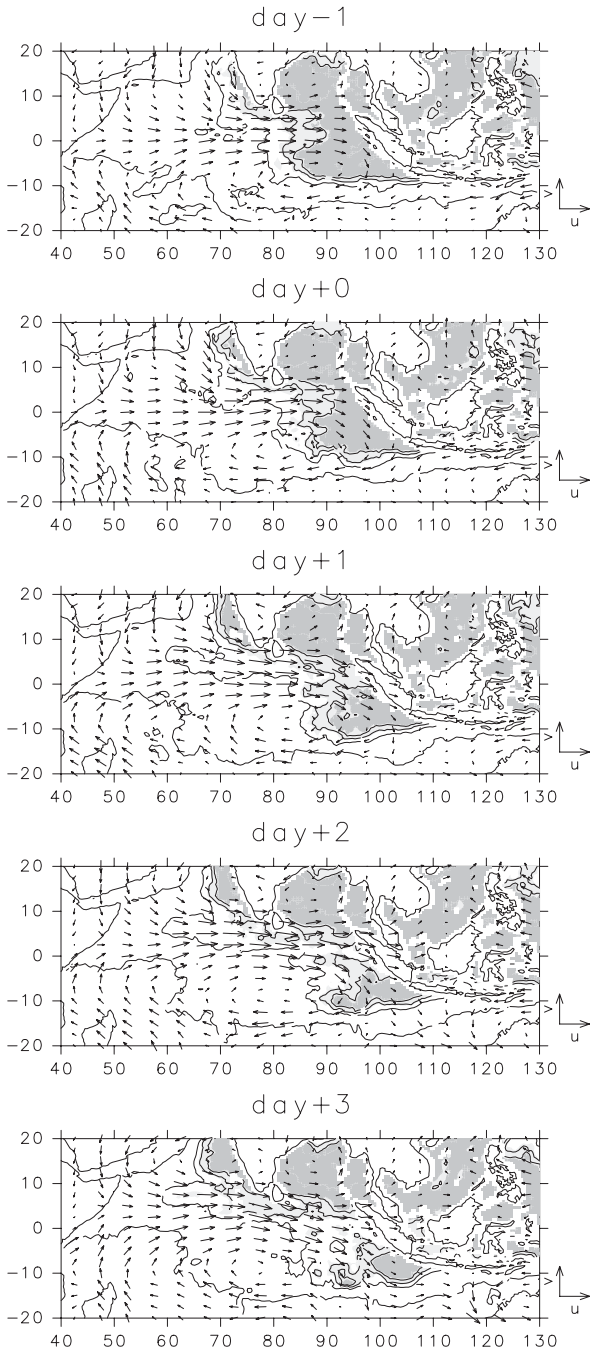

Fig. 7. Horizontal distributions of composite SSM/I PW (precipitable water) and NCEP wind at 700 hPa from Day−1 to Day+3. Shading corresponds to PW exceeding 55 mm (dark shading), and 53 mm (light shading). The contours are drawn at 55, 53, 50, and 40 mm. Unit vector shows 20 m/s.

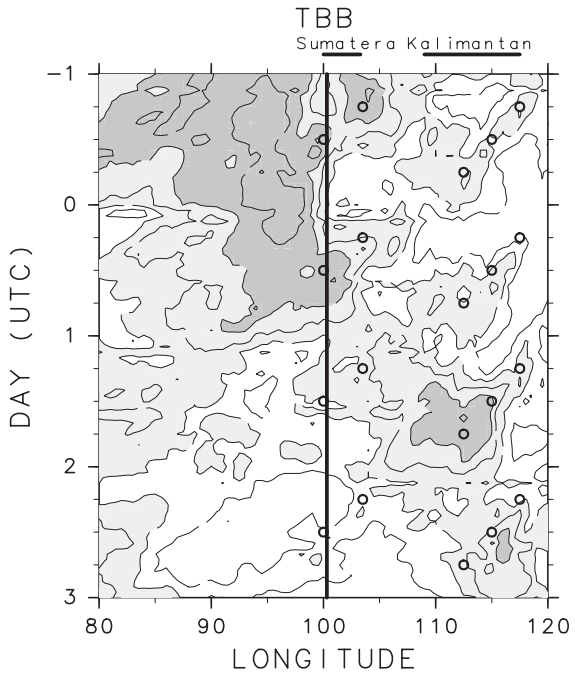

Fig. 8. Time-longitude section of composite T_{BB} averaged from 2°N to 2°S. Horizontal resolution is 0.5° and time resolution is 1 hour. A vertical line shows the location of the observation site. Dark and light shading indicates T_{BB} colder than 240 K, 260 K, respectively. The contour interval is 10 K. Two lines in the upper figure show the ranges of Sumatera and Kalimantan Islands. Remarkable diurnal variations at some locations are indicated by circles: every 06 UTC (13 LST) for 103.5°E and 117.5°E, every 12 UTC (19 LST) for 100°E and 115°E, every 18 UTC (01 LST) for 112.5°E.

Day+3, and the wind over Kalimantan switched from easterly to westerly following the passage of the cloud system.

Figure 8 shows a time-longitude section of composite T_{BB}. Data are averaged from 2°S–2°N. Horizontal resolution is 0.5° and time resolution is 1 hour. The vertical line shows the location of the observation site. High cloud tops colder than 240 K were observed over the Indian Ocean for the first 2 days, over Sumatera at around 12–18 UTC (19–01 LST of the following day) on Day+0, over the strait between Sumatera and Kalimantan Islands at 00–12 UTC (07–19 LST) on Day+1, and over

Kalimantan by 18 UTC (01 LST of the following day) on Day+1. Propagation speed was 8–10°/day (10–13 m/s). T_{BB} colder than 260 K, which corresponded to heights around 7 km, disappeared 1 day after the passage of the cloud system. Figure 8 also shows the local time dependence of cloud development. Remarkable diurnal variations are indicated by circles in Fig. 8. A clear diurnal signal in the westward propagation appeared over Kalimantan. High (cold) cloud tops appeared near 118°E at 06 UTC (13 LST), and dissipated near 112°E at 18 UTC (01 LST). A diurnal signal also appeared over Sumatera. High cloud tops appeared near 103°E at 06 UTC (13 LST), and near 100°E at 12 UTC (19 LST). Diurnal signals could be identified even in the eastward propagating cloud system. An influence of diurnal circulations was implied in this area.

Figure 9 shows back trajectories to reveal the origin of the dry air. Three-dimensional winds from the NCEP reanalysis data were used to determine the initial location of dry air parcels. The time step was 1 hour; a linear interpolation of the original 6-hourly data yielded hourly data. Back trajectories started from 700 hPa at (100°E, 0°N) at 00 UTC on Day+2 for each dry event. All trajectories originating at around 600 hPa, and they were confined between 10°S and 10°N in the east of 65°E.

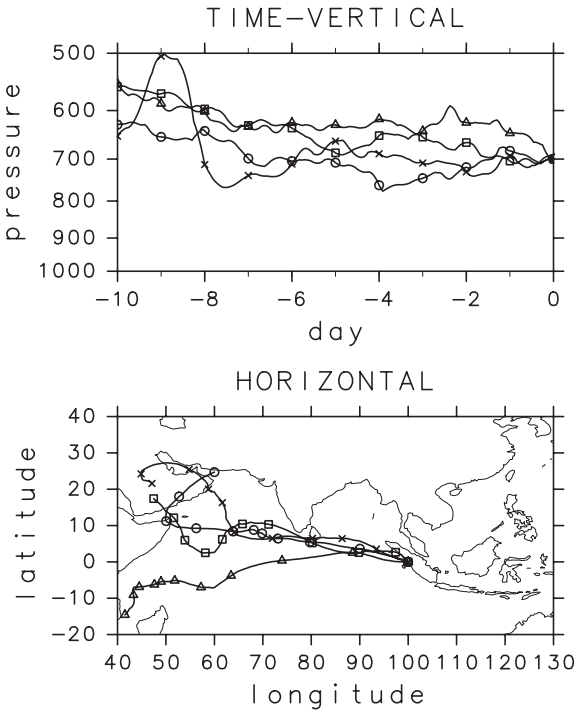

Fig. 9. Back trajectories up to 10 days start from 700 hPa at (0°N, 100°E) at 00 UTC on Day+2 for each dry event. The curves with circles, crosses, squares and triangles are the trajectories on 7 Oct 1998, 30 May 2001, 9 June 2001 and 8 May 2004, respectively.

4.2 Observational results

Sections 3 and 4.1 suggest a link between eastward-propagating cloud systems and dry events. As a cloud system propagates from the Indian Ocean to Kalimantan Island, sounding observations reflect changes following the passage of the cloud system. Such structure suggests one huge cloud system. Thus, the time axis of figures in this section is reversed, so the results shown are for the structure of an eastward-propagating cloud system.

Figure 10a is a time-height section of composite relative humidity. Prior to the passage of the cloud system, the lower troposphere had high humidity on Day−1. After the convective period, the lower troposphere dried out as the upper troposphere, above 5 km, moistened on Day+1 and Day+2. A layer with humidity drier than 50% appeared 1 day after the convective period. The layer moved upward at 1 km/day. In the moist layer, humidity increased during the night (12, 18 UTC or 19, 01 LST). Humidity below the dry layer increased as a boundary layer developed.

Figure 10b shows a time-height section of composite zonal wind. Vertical wind shear intensified after the active convection. Strong westerly wind, more than 10 m/s, appeared in the layer of 1.5–3 km at 12 UTC on Day+0, and the layer rose by around 1 km at 12 UTC on Day+0. The strong westerly wind persisted for 2 days.

Figure 11a shows a time-height section of composite specific humidity. Specific humidity below 2 km was the largest at 06–12 UTC (13–19 LST) on Day−1 before the cloud system passed. Specific humidity between 3 and 5 km was the largest at 12–18 UTC (19–01 LST of the following day) on Day+0 during the disturbed period. Specific humidity in the dry layer, between 3 and 5 km, decreased 2–4 g/kg

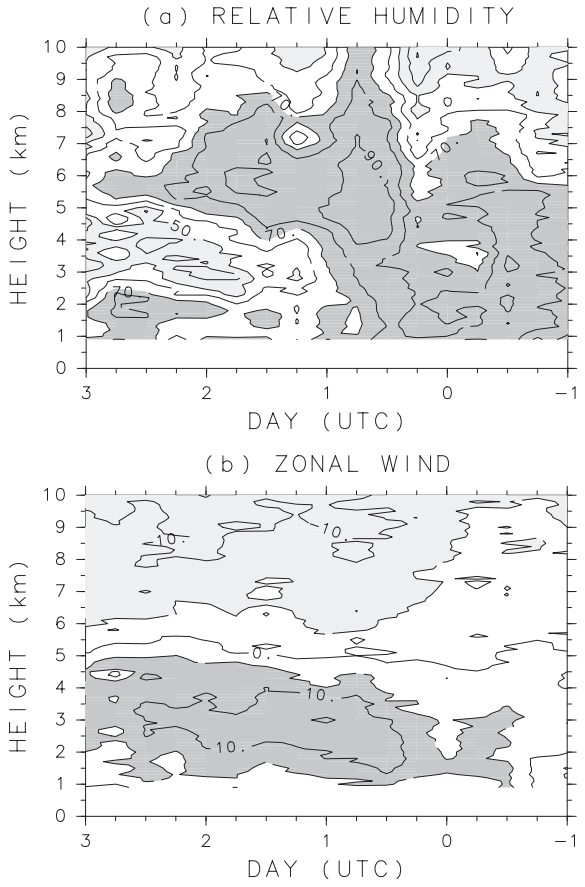

Fig. 10. (a) Time-height section of composite relative humidity. Dark and light shading indicates regions with humidity more than 70% and less than 50%, respectively. Contours are drawn every 10%. (b) Time-height section of composite zonal wind. Dark and light shading represents westerly winds exceeding 5 m/s, and easterly winds exceeding 5 m/s, respectively. Contours are drawn every 5 m/s.

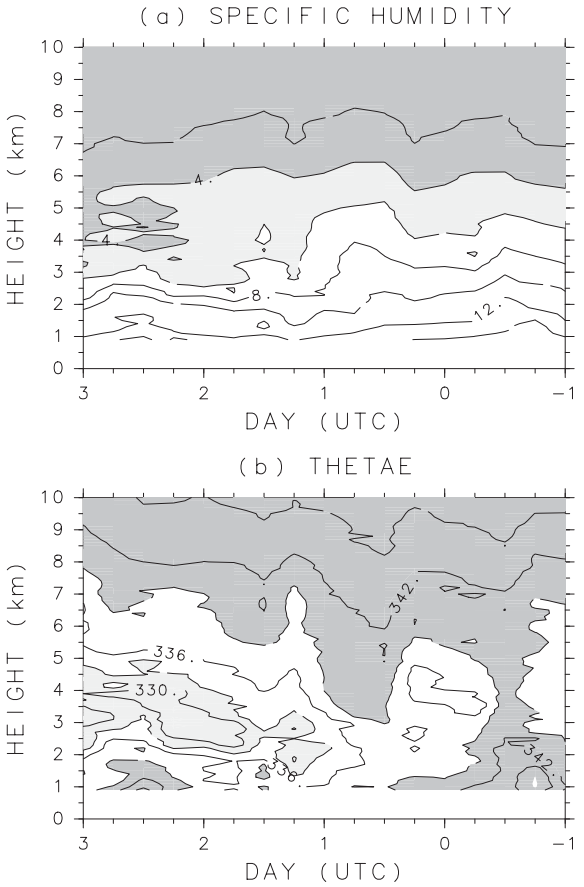

Fig. 11. (a) Time-height section of composite specific humidity. Dark and light shading indicates specific humidities less than 4 g/kg and that less than 6 g/kg, respectively. Contours are drawn every 2 g/kg. (b) Time-height section of composite equivalent potential temperature. Dark and light shading indicates θ_e more than 339 K, and less than 333 K, respectively. Contour interval is 3 K.

after the convection. Strong vertical gradient was present between 2 and 3 km on Day+1 and Day+2. Specific humidity below the dry layer increased at 12–18 UTC (19–01 LST of the following day) on Day+2 as a boundary layer developed. Specific humidity had a distinct diurnal cycle, peaking between 12 and 18 UTC (19 and 01 LST of the following day) in the upper troposphere.

Figure 11b shows a time-height section of composite equivalent potential temperature or θ_e. High θ_e values occurred near the ground; the atmosphere was potentially unstable on Day−1. The atmosphere stabilized after the convection between 12 UTC (19 LST) on Day+0 and 06 UTC (13 LST) on Day+1. Low θ_e appeared in the dry layer on Day+1 and Day+2. Near the ground, θ_e increased at 12 UTC (19 LST) on Day+1, and at 12 UTC (19 LST) on Day+2. In the upper troposphere, θ_e had a clear diurnal variation with a minimum at 06 UTC (13 LST), and a maximum at 12 UTC (19 LST).

Figure 12a shows a time-height section of

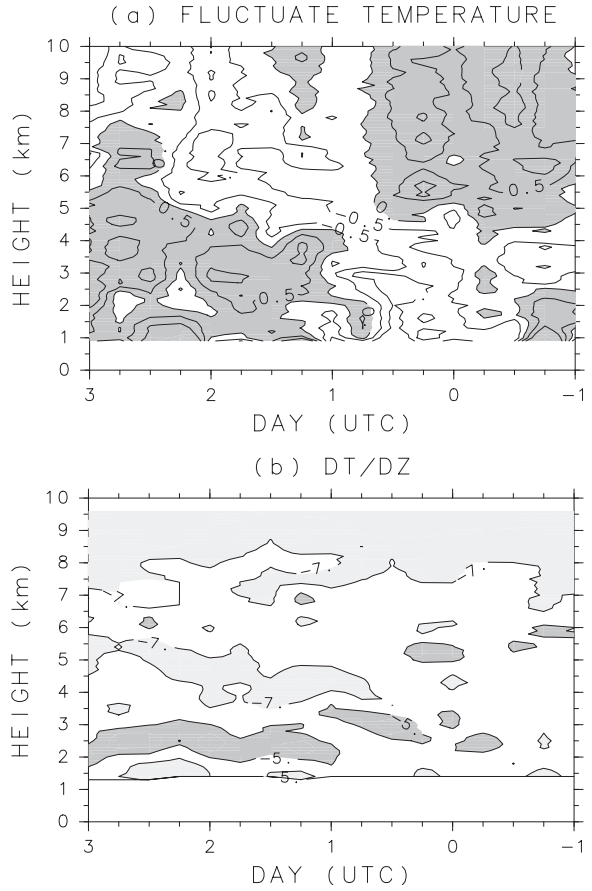

Fig. 12. (a) Time-height section of composite temperature anomalies, which were computed relative to the average profile during the analysis period. Dark shading indicates a positive anomaly, and the contour interval is 0.5 K. (b) Time-height section of a composite vertical temperature gradient. Dark shading represents stable layers (gradient larger than −5 K/km) and light shading represents unstable layers (gradient smaller than −7 K/km).

composite temperature anomalies, which were computed relative to the average profile during the analysis period. The atmosphere above 5 km was anomalously warm before the passage of the cloud system. During the disturbed period on Day+0, the atmosphere below 5 km was anomalously cold. After the disturbed period, the lower atmosphere warmed, and the upper atmosphere cooled on Day+1 and Day+2. Anomalously cold air was present between 4 and 6 km, just above the warm layer.

Figure 12b shows a time-height section of a composite vertical temperature gradient. Before the passage of the cloud system, weak stable layers appeared around 5–6 km, but they did not appear in all the events. During the disturbed period, a stable layer from 2 to 3 km penetrated into the region of active convection on Day+0. After the convection, a stable layer appeared at the bottom of the dry layer, and there was an unstable layer at the upper boundary of the dry layer on Day+1 and Day+2. Near the ground, unstable layers forced by solar heating appeared around 06 UTC (13 LST) each day.

Figure 13 shows composite surface data. The surface data are 3-hourly, except for rainfall. Rainfall amounts represent accumulation during the previous 6 hours. Composites of surface pressure and temperature were computed using deviations from averages, between 00 UTC on Day−1 and 00 UTC on Day+3. Surface pressures had a clear semidiurnal variation, because of the atmospheric tide. Daily pressure on Day+0 was about 1 hPa higher than on other days. Surface temperature and humidity also showed distinct diurnal variation. The raise of temperature in the daytime (around 06 UTC or 13 LST) was weak on Day+0, and gradually increased on Day+1 and Day+2. This is consistent with stormy weather on Day+0 and clearing afterward. High humidity on Day−1 and Day+0 corresponded to rainy conditions on those days. Daytime humidity at around 06 UTC (13 LST) decreased on Day+1 and Day+2 under the dry layer, which suggests vertical transport of upper dry air by mixing, in addition to the temperature increase. Rain fell on Day−1 and Day+0, primarily in the afternoon (06–18 UTC or 13–01 LST). Rain was not observed on Day+1 or Day+2. Heavy rainfall, exceeding 100 mm/6 hr, fell on 5 May 2004 at Padang. In addition, strong wind gusts occurred at Padang before the rainfall on 5 and 6 May 2004. Cloud systems can be accompanied by severe weather.

To summarize the results shown by Figs. 10–13, Fig. 14 schematically shows the structure of an eastward-propagating cloud system along the Equator. The lower troposphere in the convective region was anomalously cold (Fig. 12a). A stable layer (gradient less than −5 K/km) penetrated into the convective region, a region

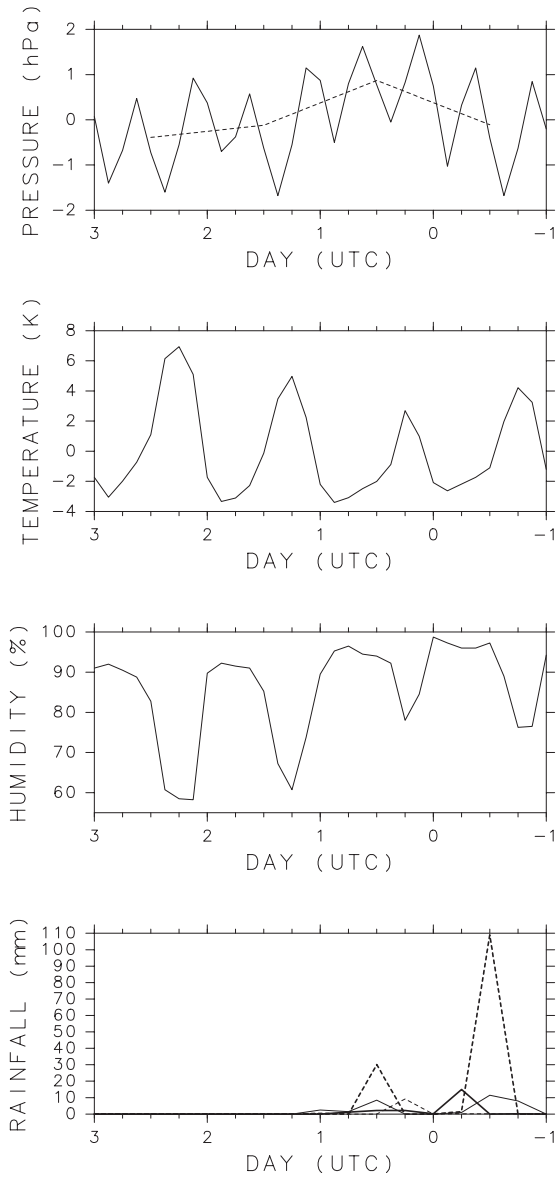

Fig. 13. Time series of 3-hourly surface pressure, temperature, humidity and 6-hourly rainfall. Data except for rainfall are composites of four dry events. Composites of pressure and temperature were computed using deviations from averages during 00 UTC Day−1 and 00 UTC Day+3. The dotted line in pressure shows the daily average. Thin solid, thin dotted, thick solid, and thick dotted lines in rainfall were observed in October 1998, May 2001, June 2001 and May 2004, respectively. The 6-hourly rainfall values are accumulations from the previous six hours.

characterized by high surface pressures and strong westerly winds. The westerly wind descended into the convective region, which may have been forced by cooling associated with sublimation, or melting of ice particles, or evaporation of rain. Anomalously cold air at the base of the wet region (Fig. 13a) supports this hypothesis. A dry region with relative humidity less than 50%, which appeared in the westerly layer 1 day after the convection, had temperature anomalies exceeding 0.5 K (Fig. 12a), although equivalent potential temperature was low, less than 333 K. There was a stable layer at the base of the dry layer (Fig. 12b). The weather in the dry and stable layers was fair with no rain (Fig. 13). Boundary layer development under the stable layer is implied by the warm, wet air and daytime destabilization (Figs. 10a, 11, and 12). Easterly winds in the upper troposphere also strengthened after the convection passed (Fig. 10b). High humidity appeared in the region of easterly winds between 5 and 8 km (Fig. 10a). Moist air between 5 and 8 km gradually cooled after the rain stopped. Regions of higher humidity aloft may have been remnants of convective towers that were advected by the easterly wind. The relative humidity increased at night (12–18 UTC, or 19–01 LST of the following day), perhaps because of greater radiative cooling.

5. Discussion

Low PW air over the Indian Ocean approached Sumatera (Fig. 7) as a dry event occurred there. The dry event appeared in the layer with westerlies the day after the strong westerly winds began (Fig. 10), suggesting the importance of horizontal advection by the westerly wind. Similar dry events in the equatorial western Pacific were recognized, and investigated as dry intrusions during TOGA COARE. Similarities and differences to features over Sumatera are discussed.

Two features were similar in the following points: (1) the levels of dry air and (2) the effect of dry air on the convection. Dry layers in this study were 2–5 km (Fig. 10a), which is similar to dry events observed in the western Pacific (Parsons et al. 1994; Numaguti et al. 1995; Yoneyama and Fujitani 1995). The level was low enough to cause a distinct decrease in PW, so dry intrusions can be analyzed in the PW dis-

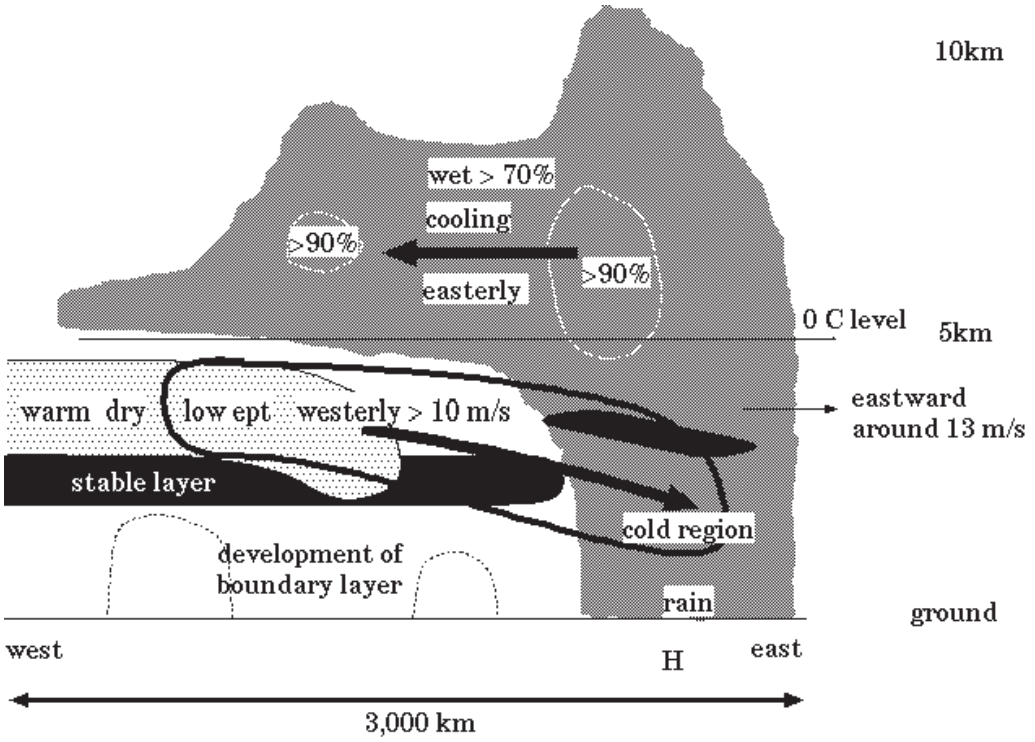

Fig. 14. A schematic diagram of the structure of an eastward propagating synoptic-scale cloud system along the equator. The cloud outline (dark shading) corresponds to relative humidity exceeding 70%. Light shading correspond to the dry layer with relative humidity less than 50%. Stable layers, in which the temperature gradient exceeded −5 K/km, are black. The thick contour denotes regions where westerly winds exceeded 10 m/s; vectors show the wind direction. 'H' at the bottom of the figure denotes high pressure. The horizontal scale was estimated by the propagating speed of the cloud system.

tribution (Fig. 7). Precipitation did not occur during the dry events (Fig. 13). Numaguti et al. (1995) and Mapes and Zuidema (1996) suggested that convective suppression is due to a stable layer at the base of dry air. A distinct stable layer was observed at the base of the dry layer in our cases (Fig. 12b). They also suggested that entrainment of the dry air forces a decrease in buoyancy. Convective suppression may also be related to the dry air at the surface, that will cause the lifting condensation level to rise (Fig. 13).

Dry events over Sumatera occurred after lower tropospheric westerly winds intensified (Fig. 10). This sequence of events is similar to a dry event described by Yoneyama and Fujitani (1995). DeMott and Rutledge (1998) described a dry event during a period of strong surface westerlies. Sheu and Liu (1995) found a correlation between westerly wind bursts and low PW, but they suggested that a dry event was triggered by a mid-latitude cold surge before the first westerly wind burst. However, the wind direction associated with dry events was not distinct during TOGA COARE (e.g., Figs. 3 and 6 of Numaguti et al. 1995). Note that some dry events were distinctly associated with easterly winds (Sheu and Liu 1995; Yoneyama 2003).

Back trajectory analyses in our study showed that the dry air originated over the western equatorial Indian Ocean (Fig. 9). In contrast, dry air observed during TOGA COARE originated over higher latitudes (Numaguti et al. 1995; Yoneyama and Fujitani 1995; Sheu and Liu 1995), or over the eastern Pacific (Yoneyama 2003). The vertical profile of humidity over the Indian Ocean is not well known, and the accuracy of the objective analysis of humidity may suffer from the lack of observations.

However, mid-levels of the atmosphere over the western equatorial Indian Ocean are drier than over the eastern equatorial Indian Ocean. The western part of the Indian Ocean is in the subsidence region of the Walker circulation and is generally convectively inactive. Moistening of mid-levels by convection is therefore considered to be rare. The horizontal gradient of PW along the equatorial Indian Ocean (Fig. 7) is consistent with this notion. In contrast, the TOGA COARE region is located east of the warm pool region, so the atmosphere is generally moister to the west. Back-trajectory results (Fig. 9), the sloping layer of westerly winds (Fig. 10b), and the warm anomaly in the dry layer (Fig. 12a), all suggest that gradual sinking motion of middle level air also contributes to lower specific humidity. The subsidence of 100 hPa per 10 days (Fig. 9), and θ_e decrease of around 6 K per day in the dry layer (Fig. 11b) can be explained by longwave radiative cooling.

Eastward-propagating synoptic-scale cloud systems (Fig. 8) were associated with the dry events, and precipitation fell before the dry events (Fig. 13). Numaguti et al. (1995) noted that rainfall occurred several days before the dry events, but no studies using data during TOGA COARE have related dry events to cloud systems. Recently, Roca et al. (2005) indicated a relation between dry intrusions and rainfall in West Africa.

The observed cloud systems have some features of Kelvin waves. The high surface pressure, and near-surface westerly winds, were nearly in phase (Fig. 14). The latitudinal extent of 10°N–10°S (Fig. 6) was similar to the deduced equatorial radius of deformation (Takayabu 1994). The observed phase speed (around 13 m/s) was also similar to past studies. Wheeler et al. (2000) and Straub and Kiladis (2002) described zonal-height sections of convectively-coupled Kelvin waves, from composites of reanalysis dataset, and rawinsondes observed in the eastern Pacific, respectively. The lower atmosphere cooled during the disturbed period, and the upper atmosphere cooled after the disturbed period, similar to Fig. 12a. The descending westerly wind anomalies toward the convective region, dry anomalies in the westerly anomalies, and wet anomaly region above the dry anomaly region in their figures are also similar to the structure of our study (Figs. 10a, b).

Other eastward-propagating cloud systems independent of dry intrusions yet with similar phase speeds and horizontal scales were observed at the observation sites (not shown). Such systems do not always follow dry intrusions, or even strong westerly winds, so dry intrusions or strong westerly winds are not necessary for the steady eastward propagation. The observed cloud system is one kind of eastward propagating synoptic-scale cloud systems.

The observed cloud system (Fig. 14) resembles a squall line (e.g., Houze 2004) in appearance, though squall lines have smaller scales (typically up to several hundred kilometers) than the cloud systems described in our study, which scale to more than 1000 km. For example, there were two similar airflows in the rear part: a descending rear inflow (westerly wind) below the 0°C layer, and front-to-rear flow (easterly wind) above the 0°C layer. The descending westerly winds were characterized by low equivalent potential temperature, and the easterly wind advected humid air. High surface pressure occurred during the period of active convection.

Composite analysis in the 700 hPa wind field (Figs. 7 and 8) revealed a stationary Matsuno-Gill pattern over the Indian Ocean and Indonesia. The eastward-propagating cloud systems near the Equator seem to overlay the standing wave. There is a hypothesis to consider stationary heating as a forcing source of MJO (e.g., Zhang and Hendon 1997), but the dry events in our study appeared in the various phases of MJOs (see, Section 3). The relationship between dry events and MJOs is beyond the aim of this study.

Observed rainfall occurred mostly in the afternoon (06–18 UTC or 13–01 LST of the following day; Fig. 13), timing that is similar to rainfall produced by diurnal disturbances. Cloud development over Sumatera and Kalimantan Islands also showed local time dependence (e.g., Mori et al. 2004; Sakurai et al. 2005, for Sumatera Island) even in the synoptic-scale disturbances (Fig. 8). They imply that diurnal-scale systems have an influence on synoptic-scale cloud systems. Figures 8 and 13 also represent that even local convections on diurnal timescales were suppressed during the dry events.

6. Conclusion

Dry events that sometimes appear over Sumatera manifest as a dry layer, between 2 and 5 km. Four dry events occurred in the westerly wind field after the westerly wind intensified to more than 10 m/s in the lower troposphere. Strong westerlies appeared as an eastward-propagating synoptic-scale cloud system passed through.

Common features of the dry events were highlighted by a composite analysis. The large-scale wind field showed a stationary Matsuno-Gill pattern over the Indian Ocean and Indonesia. A cloud system overlaying the stationary wave propagated eastward, with the latitudinal scale of 10°S–10°N; 700-hPa westerly winds followed the cloud system. The longitudinal scale of the cloud system, measured as the area where T_{BB} was colder than 260 K, was 1000 km. Propagation speed was around 13 m/s. Low values of PW over the Indian Ocean extended eastward, following the westerly wind. Dry events were caused by dry intrusions of westerly wind. The dry air originated over the equatorial western Indian Ocean.

The structure of the eastward propagating synoptic-scale cloud system was estimated by soundings. The structure of the cloud system was similar to the structure of squall lines in appearance. The cloud systems also displayed properties of a Kelvin wave: they propagated eastward along the Equator and showed an in-phase relation between the high surface pressure and lower tropospheric westerly wind.

The observed eastward-propagating synoptic-scale cloud system produced rain as it passed the observation site, and suppressed convection in the rear part of the cloud system. A systematic weather transition occurred in equatorial regions as the cloud system moved. Tropical weather forecasts may be improved in the future studies by considering these cloud systems and how they relate to the MJO.

Acknowledgement

The first author thanks Drs. Shinjiro Kanae at the Research Institute for Humanity and Nature, and Taiichi Hayashi at Kyoto University (Kyoto-U) for providing a good environment in which to continue this study. Drs. Kunio Yoneyama at the Japan Agency for Marine-Earth Science and Technology (JAMSTEC), Tetsuo Nakazawa at the Meteorological Research Institute, and Atusi Numaguti at Hokkaido University (Hokkaido-U) provided valuable comments. We appreciate good discussions with Drs. Hisayuki Kubota and Qoosaku Moteki at JAMSTEC, Tetsuya Takemi at Tokyo Institute of Technology, and Mr. Satoru Yokoi at Kyoto-U. Drs. Masatomo Fujiwara at Hokkaido-U and Shin-Ya Ogino at JAMSTEC participated in valuable discussions in the early stage of this study. We also thank the Editor (Dr. Jun Matsumoto) and two anonymous reviewers for their help to improve this paper. The observation site, 'Kototabang', was constructed and maintained through the efforts of Drs. Susumu Kato and Shoichiro Fukao at Kyoto-U, and members of the Research Institute for Sustainable Humanosphere (RISH), Kyoto-U. Rawinsonde observations were conducted in cooperation with the Agency for the Assessment and Application of Technology (BPPT), Indonesia, the Indonesian Meteorological and Geophysical Agency, the Institute of Observational Research for Global Change JAMSTEC, RISH Kyoto-U, and Kobe University. Rawinsonde observations in April–May 2004 were conducted as part of the joint project between Kyoto-U Active Geosphere Investigations for the 21st Century COE and BPPT Indonesia, and the joint project between Japan and the National Institute of Aeronautics and Space, Indonesia, called Coupling Processes in the Equatorial Atmosphere (CPEA). CPEA is supported by a Grant-in-Aid for Scientific Research on Priority Area-764 from the Ministry of Education, Culture, Sports, Science, and Technology (MEXT) of Japan. The figures in this paper were drawn using the GFD-DENNOU Library.

Appendix

Two types of Vaisala rawinsonde were used to produce soundings in 2004. The total sounding period were during 00 UTC 10 April–12 UTC 09 May 2004. Older RS80-15G models were used in the latter half of the period (12 UTC 26 April–12 UTC 09 May). Some studies (e.g., Fujiwara et al. 2003; Nakamura et al. 2004) have noted a dry bias at lower altitudes by old RS80-15G models using A-Humicap humidity sensors. A humidity correction was

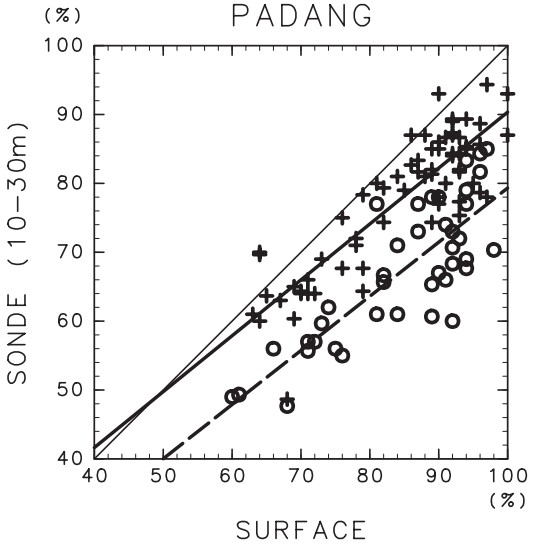

Fig. A1. Scatter plot of surface relative humidity (horizontal axis) vs. 10–30 m average relative humidity observed by rawinsondes (vertical axis). Pluses and a thin solid regression line denote data from new H-Humicap sensors on RS80-15GH rawinsondes. Circles and a dashed regression line denote data from old A-Humicap sensors on RS80-15G rawinsondes.

therefore warranted for observations in 2004, to improve quality and to standardize observations before and after 26 April. A simplified version of the method of Lucas and Zipser (2000) was applied. The humidity correction used the surface humidity value that was observed with other surface instruments and input as a first value in the rawinsonde data. This method is convenient, because corrections can be made using sounding data only. Figure A1 is a scatter plot of surface relative humidity vs. 10- to 30-m average relative humidity observed by rawinsondes. Pluses denote data from new H-Humicap sensors on the RS80-15GH radiosondes used until 00 UTC on 26 April 2004. Circles denote results using data from old A-Humicap sensors on RS80-15G models used after 12 UTC on 26 April 2004. Surface humidity was observed by a thermohygrograph with a sun screen throughout the sounding period. Solid and dashed lines are regression lines for the pluses and circles, respectively. We observed good correlation between surface instruments and both types of sensor. The figure shows a 10% dry bias for the old A-Humicap sensors as compared to the new H-Humicap sensors. Fujiwara et al. (2003) noted that humidity observed using the new H-Humicap sensors had no bias when compared with data from chilled mirror hygrometers. Therefore, the humidity correction was applied only to data retrieved from old A-Humicap sensors. The correction process included the following steps: 1) An estimated value of surface humidity was calculated from the dashed regression line. 2) The humidity difference between the two regression lines for the estimated value was added as a correction value. Corrections were conducted only for humidity exceeding 40% and for pressure exceeding 500 hPa, because of uncertainties in the corrections necessary for lower humidity values and higher heights. Correction values were reduced linearly between 40 and 50% and between 500 and 700 hPa to avoid discontinuities. The few values that exceeded 100% were set to 100%.

References

Brown, R.G. and C. Zhang, 1997: Variability of mid-tropospheric moisture and its effect on cloud-top height distribution during TOGA COARE. *J. Atmos. Sci.*, **54**, 2760–2774.

DeMott, C.A. and S.A. Rutledge, 1998: The vertical structure of TOGA COARE convection. part 2: modulating influences and implications for diabatic heating. *J. Atmos. Sci.*, **55**, 2748–2756.

Dunkerton, T.J. and F.X. Crum, 1995: Eastward propagating 2- to 15-day equatorial convection and its relation to the tropical intraseasonal oscillation. *J. Geophys. Res.*, **100**, 25 781–25 790.

Fujiwara, M., M. Shiotani, F. Hasebe, H. Vomel, S.J. Oltmans, P.W. Ruppert, T. Horinouchi, and T. Tsuda, 2003: Performance of the meteolabor 'Snow White' chilled-mirror hygrometer in the tropical troposphere: Comparisons with the Vaisala RS80 A/H-Humicap sensors. *J. Atmos. Oceanic Technol.*, **20**, 1534–1542.

Gill, A.E., 1980: Some simple solutions for heat-induced tropical circulation. *Quart. J. Roy. Meteor. Soc.*, **106**, 447–462.

Hadi, Tri W., T. Tsuda, H. Hashiguchi, and S. Fukao, 2000: Tropical sea-breeze circulation and related atmospheric phenomena observed with L-band boundary layer radar in Indonesia. *J. Meteor. Soc. Japan*, **78**, 123–140.

———, T. Horinouchi, T. Tsuda, H. Hashiguchi, and

S. Fukao, 2002: Sea-breeze circulation over Jakarta, Indonesia: A climatology based on boundary layer radar observations. *Mon. Wea. Rev.*, **130**, 2153–2166.

Hendon, H.H. and K. Woodberry, 1993: The diurnal cycle of tropical convection. *J. Geophys. Res.*, **98**, 16 623–16 637.

Houze, R.A., S.G. Geotis, F.D. Marks, and A.K. West, 1980: Winter monsoon convection in the vicinity of north Borneo. part 1: structure and time variation of the clouds and precipitation. *Mon. Wea. Rev.*, **109**, 1595–1614.

———, 2004: Mesoscale convective systems. *Rev. Geophys.*, **42**, RG4003.

Johnson, R.H., P.E. Ciesieleski, and J.A. Cotturone, 2001: Multiscale variability of the atmospheric mixed layer over the western Pacific warm pool. *J. Atmos. Sci.*, **58**, 2729–2750.

Kalnay, E. and Coauthors, 1996: The NCEP-NCAR 40-year reanalysis project. *Bull. Amer. Meteor. Soc.*, **78**, 437–471.

Lucas, C. and E.J. Zipser, 2000: Environmental variability during TOGA COARE. *J. Atmos. Sci.*, **57**, 2333–2350.

Madden, R.A. and P.R. Julian, 1971: Detection of a 40–50 day oscillation in the zonal wind in the tropical Pacific. *J. Atmos. Sci.*, **28**, 702–708.

——— and ———, 1972: Description of global scale circulation cells in the tropics with a 40–50 day period. *J. Atmos. Sci.*, **29**, 1109–1123.

——— and ———, 1994: Observations of the 40–50-day tropical oscillation—a review. *Mon. Wea. Rev.*, **122**, 814–837.

Mapes, B.E. and P. Zuidema, 1996: Radiative-dynamical consequences of dry tongues in the tropical troposphere. *J. Atmos. Sci.*, **53**, 620–638.

Matsuno, T., 1966: Quasi-geostrophic motions in the equatorial area. *J. Meteor. Soc. Japan*, **44**, 25–42.

Mori, S., J.-I. Hamada, Y.I. Tauhid, M.D. Yamanaka, N. Okamoto, F. Murata, N. Sakurai, H. Hashiguchi, and T. Sribimawati, 2004: Diurnal land-sea rainfall peak migration over Sumatera Island, Indonesian maritime continent observed by TRMM satellite and intensive rawinsonde soundings. *Mon. Wea. Rev.*, **132**, 2021–2039.

Murakami, M., 1983: Analysis of the deep convective activity over the western Pacific and southeast Asia. *J. Meteor. Soc. Japan*, **61**, 60–76.

Murata, F., M.D. Yamanaka, F. Fujiwara, S. Ogino, H. Hashiguchi, S. Fukao, M. Kudsy, T. Sribimawati, S.W.B. Harijono, and E. Kelana, 2002: Relationship between wind and precipitation observed with a UHF radar, GPS rawinsondes and surface meteorological instruments at Kototabang, West Sumatera during September–October 1998. *J. Meteor. Soc. Japan*, **80**, 347–360.

Nakamura, H., H. Seko, Y. Shoji, Aerological observatory, and Meteorological instruments center, 2004: Dry biases of humidity measurements from the Vaisala RS80-A and Meisei RS2-91 radiosondes and from ground-based GPS. *J. Meteor. Soc. Japan*, **82(1B)**, 277–299.

Nakazawa, 1986: Mean features of 30–60 day variations as inferred from 8-year OLR data. *J. Meteor. Soc. Japan*, **64**, 777–786.

———, 1988: Tropical super clousters within intraseasonal variations over the western Pacific. *J. Meteor. Soc. Japan*, **66**, 823–839.

Nitta, T. and S. Sekine, 1994: Diurnal variation of convective activity over the tropical western Pacific. *J. Meteor. Soc. Japan*, **72**, 627–641.

Numaguti, A., R. Oki, K. Nakamura, K. Tsuboki, N. Misawa, T. Asai, and Y.-M. Kodama, 1995: 4–5-day-period variation and low-level dry air observed in the equatorial western Pacific during the TOGA-COARE IOP. *J. Meteor. Soc. Japan*, **73(2B)**, 267–290.

Parsons, D., W. Dabberdt, H. Cole, T. Hock, C. Martin, A.-L. Barrett, E. Miller, M. Spowart, M. Howard, W. Ecklund, D. Carter, K. Gage, and J. Wilson, 1994: The integrated sounding system: description and preliminary observations from TOGA COARE. *Bull. Amer. Meteor. Soc.*, **75**, 553–567.

———, K. Yoneyama, and J.-L. Redelsperger, 2000: The evolution of the tropical western Pacific atmosphere–ocean system following the arrival of a dry intrusion. *Quart. J. Roy. Meteor. Soc.*, **126**, 517–548.

Ramage, C.S., 1968: Role of a tropical 'maritime continent' in the atmospheric circulation. *Mon. Wea. Rev.*, **96**, 365–369.

Redelsperger, J.-L., D.B. Parsons, and F. Guichard, 2002: Recovery processes and factors limiting cloud-top height following the arrival of a dry intrusion observed during TOGA COARE. *J. Atmos. Sci.*, **59**, 2438–2457.

Roca, R., J.-L. Lafore, C. Piriou, and J.-L. Redelsperger, 2005: Extratropical dry-air intrusions into the West African monsoon midtroposphere: an important factor for the convective activity over the Sahel. *J. Atmos. Sci.*, **62**, 390–407.

Renggono, F., H. Hashiguchi, S. Fukao, M.D. Yamanaka, S.-Y. Ogino, N. Okamoto, F. Murata, B.P. Sitorus, M. Kudsy, M. Kartasasmita, and G. Ibrahim, 2001: Precipitating clouds observed by 1.3-GHz boundary layer radars in equatorial Indonesia. *Ann. Geophysicae*, **19**, 889–897.

Sakurai, N., F. Murata, M.D. Yamanaka, S. Mori, J.-I. Hamada, H. Hashiguchi, Y.I. Tauhid, T. Sribimawati, and B. Suhardi, 2005: Diurnal cycle of migration of convective cloud systems over Sumatera Island. *J. Meteor. Soc. Japan*, **83**, 835–850.

Sheu, R.-S. and G. Liu, 1995: Atmospheric humidity variations associated with westerly wind bursts during Tropical Ocean Global Atmosphere (TOGA) Coupled Ocean Atmosphere Response Experiment. *J. Geophys. Res.*, **100**, 25759–25768.

Straub, K.H. and G.N. Kiladis, 2002: Observations of a convectively coupled Kelvin wave in the eastern Pacific ITCZ. *J. Atmos. Sci.*, **59**, 30–53.

Sui, C.-H. and K.-M. Lau, 1992: Multiple phenomena in the tropical atmosphere over the western Pacific. *Mon. Wea. Rev.*, **120**, 407–430.

Takayabu, Y.N. and M. Murakami, 1991: The structure of super cloud clusters observed on 1–20 June 1986 and their relationship to easterly waves. *J. Meteor. Soc. Japan*, **69**, 105–125.

———, 1994: Large-scale cloud disturbances associated with equatorial waves. Part I: Spectral features of the cloud disturbances. *J. Meteor. Soc. Japan*, **72**, 433–448.

Webster, P.J. and R. Lucas, 1992: TOGA COARE: The coupled ocean-atmosphere response experiment. *Bull. Amer. Meteor. Soc.*, **73**, 1377–1416.

Wheeler, M. and G.N. Kiladis, 1999: Convectively coupled equatorial waves: analysis of clouds and temperature in the wave-number-frequency domain. *J. Atmos. Sci.*, **56**, 374–399.

———, ———, and P.J. Webster, 2000: Large-scale dynamical fields associated with convectively coupled waves. *J. Atmos. Sci.*, **57**, 613–640.

Yang, G.-Y. and J. Slingo, 2001: The diurnal cycle in the tropics. *Mon. Wea. Rev.*, **129**, 784–801.

Yatagai, Y. and A. Sumi, 1997: Statistical features of dry air intrusions into the equatorial ocean. *Proceedings of COARE97 conference*, 161–162.

Yoneyama, K. and T. Fujitani, 1995: The behavior of dry westerly air associated with convection observed during the TOGA-COARE R/V Natsushima cruise. *J. Meteor. Soc. Japan*, **73(2B)**, 291–304.

——— and D.B. Parsons, 1999: A proposed mechanism for the intrusion of dry air into the tropical western Pacific region. *J. Atmos. Sci.*, **56**, 1524–1546.

———, 2003: Moisture variability over the tropical western Pacific ocean. *J. Meteor. Soc. Japan*, **81(2)**, 317–337.

Zachariasse, M., H.G. Smit, P.F.J. van Velthoven, and H. Kelder, 2001: Cross-tropopause and interhemispheric transports into the tropical free troposphere over the Indian Ocean. *J. Geophys. Res.*, **106**, 28 441–28 452.

Zhang, C. and H.H. Hendon, 1997: Propagating and standing components of the intraseasonal oscillation in tropical convection. *J. Atmos. Sci.*, **54**, 741–752.